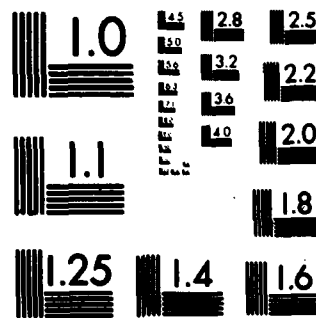AD-A091 865   IMPERIAL COLL OF SCIENCE AND TECHNOLOGY LONDON (ENGLA--ETC F/G 20/4
                IMBEDDED LONGITUDINAL VORTICES IN TURBULENT BOUNDARY LAYERS,(U)
                1980   R D MEHTA, I M SHABAKA, P BRADSHAW
UNCLASSIFIED   NL

END
DATE
FILMED
I 9
DTIC

MICROCOPY RESOLUTION TEST CHART
NATIONAL BUREAU OF STANDARDS 1963-A

IMBEDDED LONGITUDINAL VORTICES IN TURBULENT BOUNDARY LAYERS

R.D. Mehta   I.M.M.A. Shabaka and P. Bradshaw
Department of Aeronautics
Imperial College,
London, SW7 2BY

Abstract

Measurements, including all Reynolds stresses and triple products, have been made in three turbulent flows with imbedded longitudinal vortices generated by skewing of the mean flow ("secondary flow of the first kind")

(i) flow in an idealized wing-body junction

(ii) an isolated vortex in a two-dimensional boundary layer, and

(iii) a vortex pair in a turbulent boundary layer.

Selected results are presented: spatial variations of eddy diffusivities and dimensionless modelling parameters are seen to be complicated.

1. Introduction

Sufficiently strong lateral deflection ("skewing") of the mean streamlines in a shear layer can lead to the generation of discrete longitudinal vortices. The mechanism is basically inviscid, given the presence of an initial shear: this "skew-induced" vorticity should be distinguished from the generation of streamwise vorticity by Reynolds stresses, which is important only in very long, straight streamwise corners and is confined in practice to non-circular ducts. In most cases of practical interest the boundary layer and the imbedded vortex will be turbulent but the decay of the vortex under the action of Reynolds stresses is slow, because its circulation is reduced only by the effect of the spanwise component of skin friction. That is, the skew induced vortices can influence the flow for a very long distance downstream. The present paper is a description of measurements of the mean and turbulent properties of decaying vortices and vortex pairs: the process of formation (being "inviscid") does not require such detailed study as the slow decay. The configurations used are idealizations of those found in practice, but the data should be useful for developing and testing calculation methods intended for real life cases.

The most obvious case in which lateral deflection of a shear layer leads to the generation of discrete vortices is divergence of the boundary layer flowing over a surface around a tall obstacle protruding from the surface. The horseshoe vortex wrapped round the junction between a wing and a body, an axial flow turbomachine blade and a hub, or a hull and a fin, is formed in this way. A single vortex trails downstream in each wing-body corner, while downstream of the trailing edge the two vortices merge to form a pair with the "common flow"

between them directed towards the surface. Vortices can also be generated on nearly-flat surfaces, by sufficiently strong crossflow. The vortex pair on the leeward side of a body of revolution at incidence, and the bilge vortices generated near the bow of a ship with a full hull form, are two examples. A vortex pair can be formed in a sufficiently strong convergent crossflow, as in the bottom of a "S-bend" dorsal intake or the wall of a wind tunnel contraction: in this case the "common flow" is away from the surface and leads to rapid thickening of the boundary layer. The Taylor-Gortler vortices that form in laminar or turbulent boundary layer flow over concave surfaces have some points of similarity with the decaying vortices discussed above, but will not be discussed further in the present paper: detailed investigations are being carried out by the present authors' colleagues.

The experiments to be described in the present paper relate to:

(i) one leg of a horseshoe vortex in a 90 deg streamwise corner

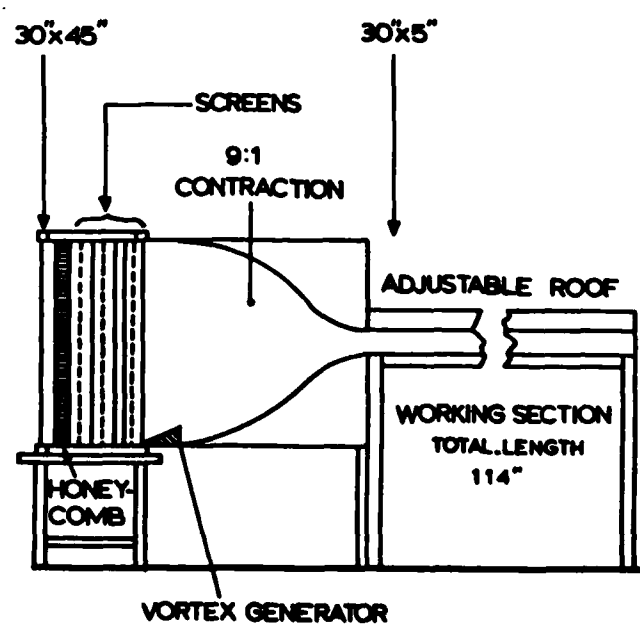(ii) an isolated vortex in the boundary layer on a flat surface, the vortex being artificially

Figure 1. Test rig (blower not shown).

(iii) vortex pairs on flat surfaces: again, the vortices are artificially generated far upstream and the "common flow" can have either sign.

2. Test rigs.

All the experiments were done in a 30 in x 5 in (762 mm x 127 mm) open circuit blower wind tunnel (Fig.1). Working section lengths up to about 3 m could be used. The nominal tunnel speed for all experiments was 100 ft/sec (30 m/s). Standard Pitot tubes, three-hole Conrad yawmeters, and conventional cross hot wire probes were used for the measurements. The fluctuating signals from hot wires were recorded on analogue magnetic tape, and later transcribed to digital magnetic tape for computer analysis, including linearization. Statistics involving both v and w components were deduced from measurements with the cross wire-probe rotated through various angles about its axis.

The corner vortex was generated by an idealized wing, spanning the 5 in height of the tunnel with its leading edge 57 in. from the working section entrance (Fig.2). The model had a half-elliptical nose 6 in.long, followed by a slab of 2 in constant thickness. Thus, pressure gradients were negligible except in the leading edge region, and there was no tendency for the vortex to drift away from the corner under the influence of pressure gradient. The boundary layer on the "body" (actually the floor of the wind tunnel) was about 1 in.thick at the leading edge.

The isolated vortices and vortex pairs on flat surfaces are generated by half-delta wings mounted in the settling chamber of the wind tunnel, as shown in Fig. 1. As the flow passes through the contraction, the circulation around the vortex is conserved, but the percentage velocity decrement in the wake of the delta-wing is very much reduced, so that at exit from the 9 to 1 two-dimensional contraction we have a concentrated vortex with nearly uniform axial velocity. (Although the contraction is two-dimensional, the vortex rapidly recovers its circular shape.) For the vortex pair experiments, two delta-wing vortex generators, set close together, are used: the vortex generator configurations were developed by flow visualization experiments in another wind tunnel before quantitative measurements began.
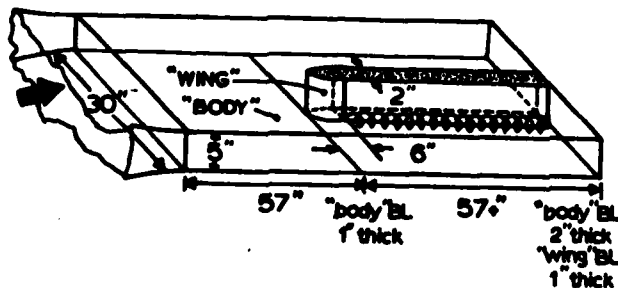

Figure 2. Wing-body junction test section.

3. Results

Some features are common to the results of all the experiments. The circulation around the isolated vortices, and even the circulation around one vortex of a pair, decreases only very slowly with downstream distance. Even vortices that are initially very small grow quite rapidly to fill the boundary layer, the growth rate being comparable with that of plumes of passive contaminants. The diameter of the corner vortex remains roughly equal to the local thickness of the body boundary layer (which is thicker than the wing boundary layer) but the region of velocity defect in the isolated vortices and vortex pair projects well outside the undisturbed boundary layer. Another feature, common to all the configurations, is the complicated behaviour of the various components of eddy viscosity, which become negative in significant regions of the flow: this implies that the use of a simply behaved eddy viscosity to predict the spreading rate of the vortex is likely to be unsatisfactory unless only gross properties are required. Unfortunately, the behaviour of the triple velocity products which appear in the Reynolds stress transport equations is also complicated, so that although calculation methods based on transport equations are needed in principle for the calculation of vortex flows, they may be difficult to develop in practice. Although this paper is not directly concerned with calculation methods, it should be pointed out that a calculation method which has been optimized for predicting secondary flows of the second kind (the "stress induced" secondary flows found in long non-circular ducts) will not necessarily be very good at predicting secondary flows of the first kind (the skew induced flows discussed in the present paper).

3.1 The corner vortex

This work is fully described by Shabaka [1] and a synoptic is given by Shabaka and Bradshaw [2]. The results are archived on magnetic tape in the Thermosciences Division, Stanford University, as part of the data set for the 1980/81 Conferences on Complex Turbulent Flows [3]. The "wing" used is shown in Fig. 2, which also gives details of the initial boundary layers. Measurements were not made in the leading edge region in which the horseshoe vortex is generated, and the measurements made at the start of the parallel section of the wing give the initial conditions from which the vortex decays.

Mean velocity contours at three streamwise positions are shown in Fig. 3. The position of the vortex centre, deduced from results presented below, is shown approximately as a guide to understanding. The distortion of the mean velocity contours by the vortex is relatively mild, but, as shown in Fig. 4, crossflow angles of several degrees are found near the wing and body surfaces. Figure 4 hints, and Fig. 5 shows plainly, that the vorticity is not a maximum at the position which Fig. 4 indicates to be the centre of the vortex but is largest near the surface of the body, where of course it consists mainly of the secondary shear dW/dy, dV/dz being comparatively small. Surface crossflow angles are large enough to be visible in surface oil flow
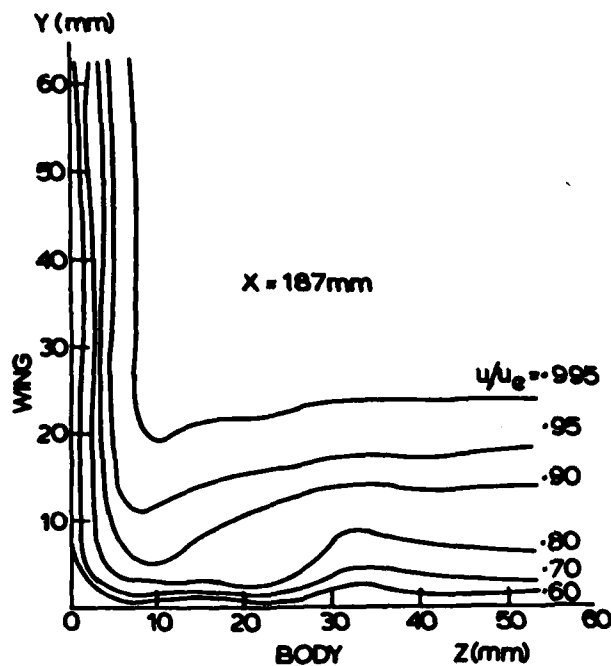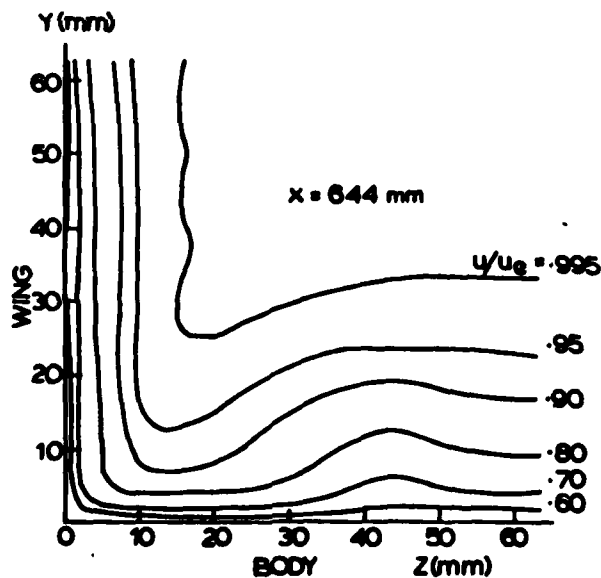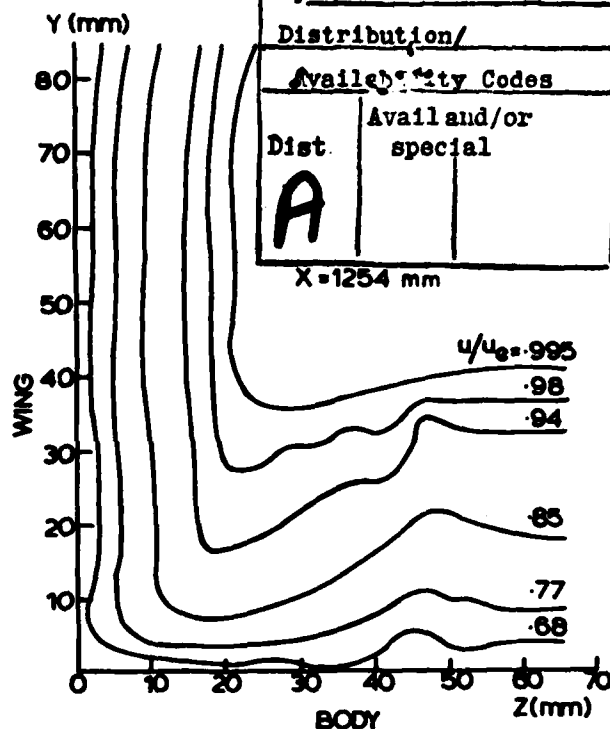
Figure 3. Streamwise velocity contours in wing-body junction flow.

(a) x=187.1 mm

(c) x=1254 mm

(b) x=644.3 mm

pictures (1). The effect of transport of x-component momentum by the vortex on the skin-friction coefficient can be deduced qualitatively from the velocity contours near the surface in Fig. 3: the velocity profiles follow the logarithmic law over significant distances, except very near the corner.
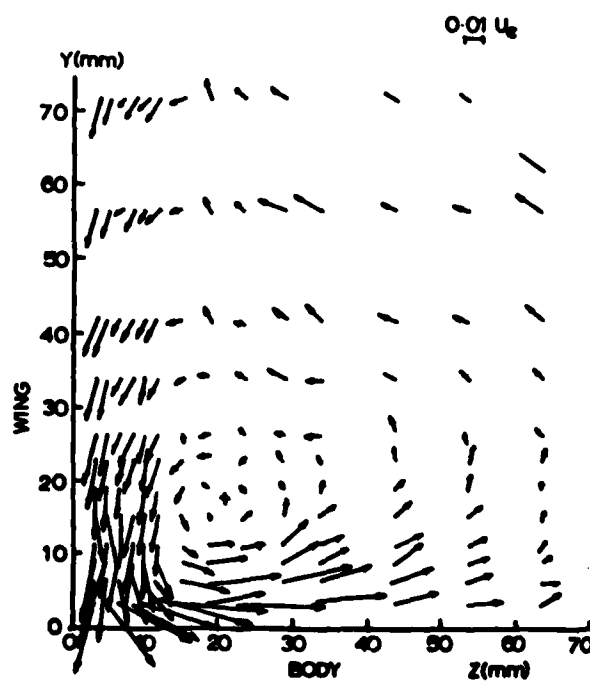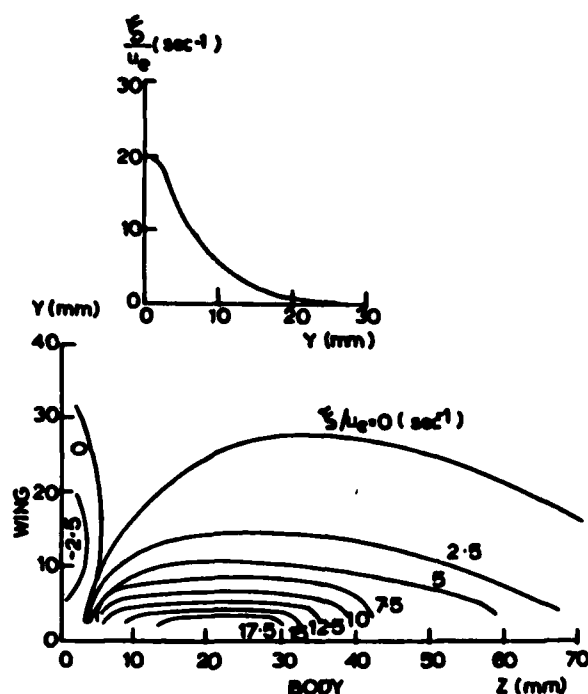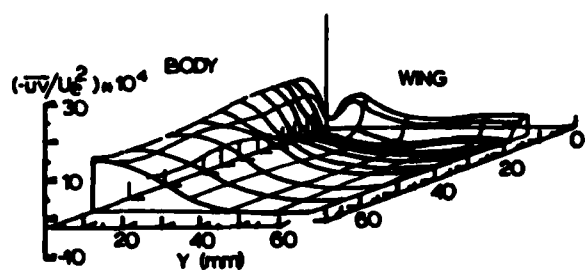
Figure 4. Secondary flow vectors at x=614 mm

Figure 5. Streamwise vorticity contours at x=614 mm

(a) $\overline{uv}$

(b) $\overline{uw}$

(c) $\overline{vw}$
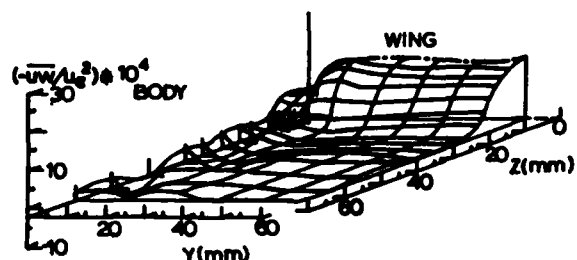
Figure 6. Reynolds stress contours at x=614 mm

Contours of turbulence intensity, of which examples are given in Ref.2, look qualitatively like the axial velocity contours. Figure 6 shows isometric views of the profiles of the Reynolds shear stresses. Far from the corner, the profiles of $\overline{uv}$ (the body shear stress) and of $\overline{uw}$ (the wing shear stress) revert to two-dimensional behaviour, but $\overline{uv}$ in particular behaves very oddly near the corner, in a way that could not be accounted for by convection of the basic boundary layer stress pattern by the secondary flow. The shear stress in the yz-plane, $\overline{vw}$, is fairly small except in the vicinity of the vortex centre, where it changes sign rapidly. The eddy viscosities defined as $-\overline{uv}/dU/dy$ and $-\overline{uw}/dU/dz$, have negative regions near the wing, and near the body, respectively: the shear stresses in the region of negative viscosity are significant, so that the transfer of axial momentum away from the corner would be seriously miscalculated in the region near the solid surfaces if an eddy viscosity based on two-dimensional boundary layer practice were used.
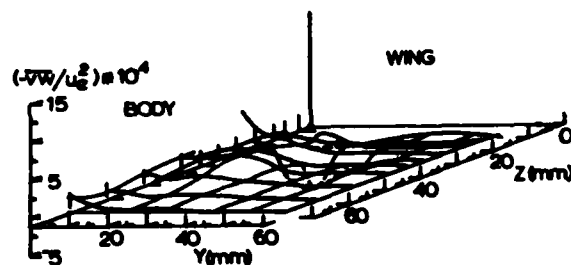
It is not possible, in a short paper to discuss the rather complicated behaviour of the rather large number of relevent triple-products. Fig. 7 shows profiles of $\overline{uv^2}$, the rate of turbulent transport of $\overline{uv}$ (the body shear stress) in the y direction (away from the body). For large values of z, results are typical of isolated boundary layers, but the profiles become greatly distorted nearer the corner, and $\overline{uv^2}$ appears to asymptote to non-zero values at y within the wing boundary layer, although values at very large y (i.e. in the two-dimensional wing boundary layer far from the body) must tend to zero.

3.2 Single isolated vortex

Figure 8 shows the axial velocity contours just downstream of the start of the working section, where the floor boundary layer is about 4 mm thick. The height of the vortex centre is expected to be at about y=10mm, and its z coordinate is obviously about 25mm (the z origin being effectively arbitrary). Figure 9 shows axial velocity contours, and secondary flow vectors about 1.3 m downstream of the start of the working section. For larger negative values of z than those shown here, the velocity contours asymptote to the approximately two-dimensional state shown for large positive z. The vortex centre is quite clearly defined, at roughly the same z position as in Fig. 8, but at about 20 mm from the surface, indicating that the vortex moves away from the surface as the boundary layer thickens. (Contours at x=1.94 m are nearly geometrically similar to those shown here.)
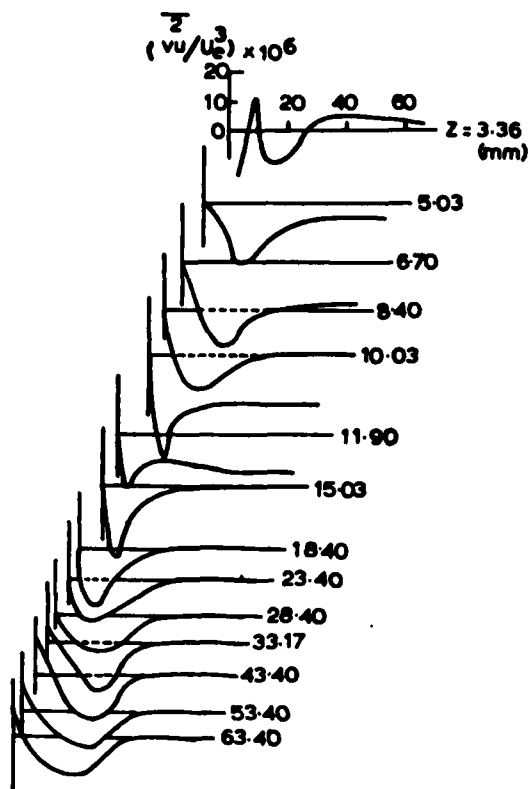
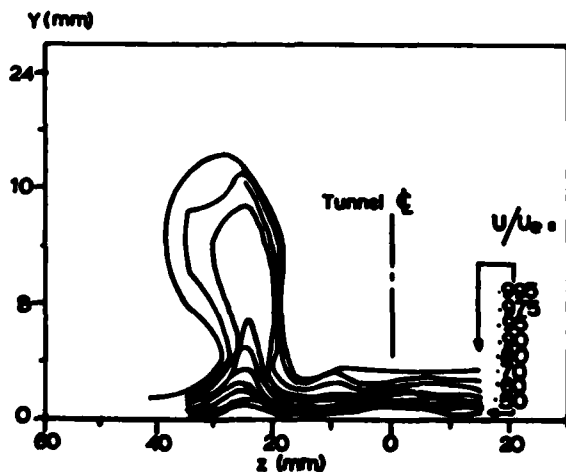Figure 7. Profiles of triple product $\overline{uv^2}$ at x=614 mm

Figure 8. Mean velocity contours in single isolated vortex at x=112 mm

As in the case of a corner vortex, maximum crossflow angles and maximum streamwise vorticity occur near the surface. However, the region of total pressure deficit in the vortex extends out to about twice the thickness of the undisturbed boundary layer; since the initial total pressure deficit in the vortex (Fig. 8) is quite small, this low total pressure fluid must have been
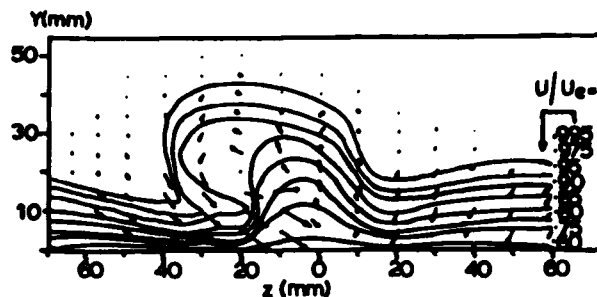

Figure 9. Mean velocity contours and secondary flow vectors at x=1332 mm.

transported from near the surface by the secondary flow, assisted by turbulent diffusion.

The effect of z-wise convection of fluid by the vortex, in an action broadly similar to the rolling of sheet metal, is simply demonstrated by the behaviour of the skin friction coefficient shown in Fig. 10: velocity profiles near the surface obey the logarithmic law at all values of z, so that the skin friction is roughly proportional to the square of the velocity at, say, y= 0.16. The skin friction profiles are qualitatively explicitable by the transfer of high momentum fluid towards the surface in the region of z=-40, and transfer away from the surface in the region of z=0 : the secondary peak in cf at z=20, corresponding to the dip in the velocity contours near this position, is more difficult to explain. The secondary velocity contours in station 9 show some hints of a second vortex, with its axis at about z=20, but it is not certain exactly how this second vortex is produced.
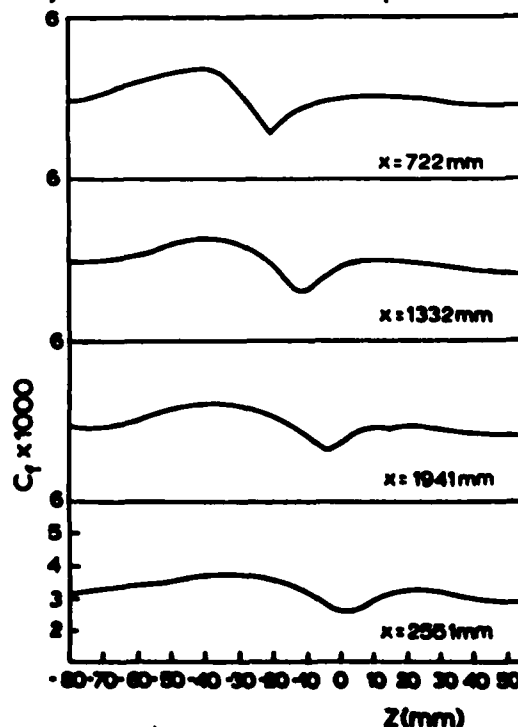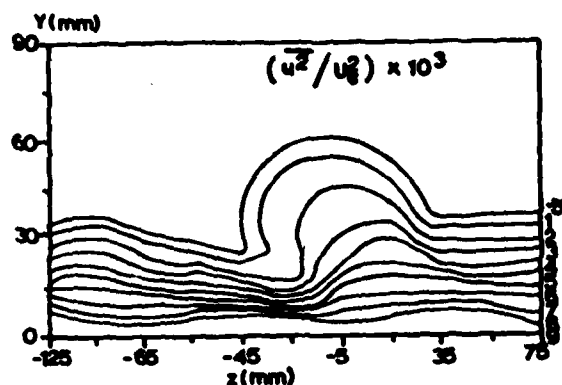

Figure 10. Skin friction in single isolated vortex.

Figure 11. Longitudinal component intensity contours.

Figure 12. Primary shear stress contours.

Figure 11 shows contours of longitudinal turbulence intensity. As in the case of the corner vortex, the intensity contours look roughly similar to the velocity contours, and this similarity extends to the v and w component intensities as well.

The $\overline{uv}$ contours shown in Fig. 12 are chosen so that the outermost approximately coincides with the edge of the undisturbed boundary layer, but it is clear that the region of significant $\overline{uv}$ within the vortex is very much smaller than that outlined by the outermost velocity contour. Bodily rotation of the fluid in the vortex, so that eddies with a contribution to $\overline{uv}$ are rotated so as to contribute to $\overline{uw}$ instead, must be responsible. Figure 13 shows that $\overline{uw}$ (zero in a two-dimensional flow) is indeed complicated. The very rapid z-wise gradient in the region of z=10 mm lines up with the position of the "tongue" in uv shown in the previous Fig. Contours of "0+" and "0-" are shown separately for clarity: in fact the zero contour has several cusps. The region of large positive $\overline{uw}$ at z=-25, where $\overline{uv}$ falls rather rapidly to zero, is in the right sense to be explained as a rotation, by the main vortex, of eddies originally contributing negatively to $\overline{uv}$. The concentrated region of negative $\overline{uw}$ near z=15 is more difficult to explain, as is that near z=-85. Figure 14 shows $\overline{vw}$, again with "0+" and "0-" contours indicated. The general shape of the contours is believed to be trustworthy, but the large negative peak at y=8, z=15 appears implausible. Eddy viscosities corresponding to these Reynolds stresses have not yet been evaluated quantitatively, but even the casual observation that $\overline{uv}$ is everywhere of the same sign, whereas the velocity gradient dU/dy reverses, clearly indicates that the eddy viscosity will be ill-behaved.

Figure 15 shows profiles of the triple product $\overline{uv^2}$. As in Fig. 7, large departures from the two-dimensional behaviour exemplified by values at large z are seen to occur.
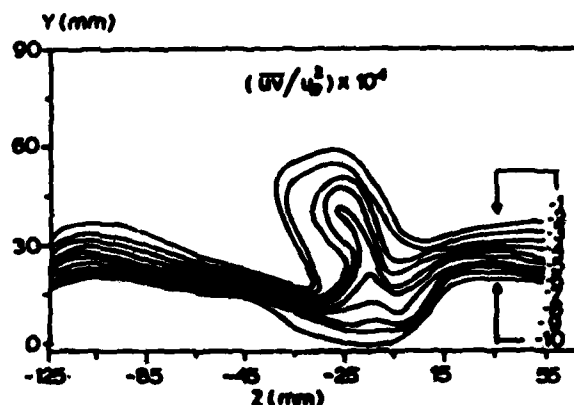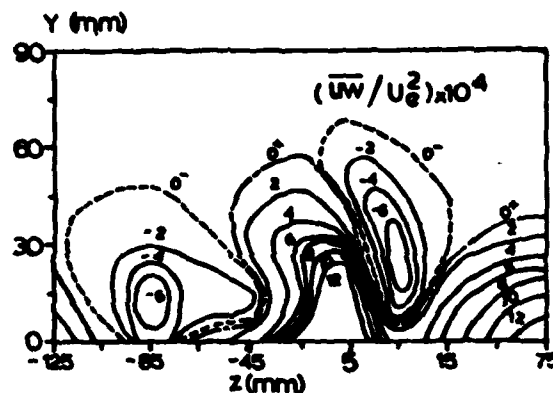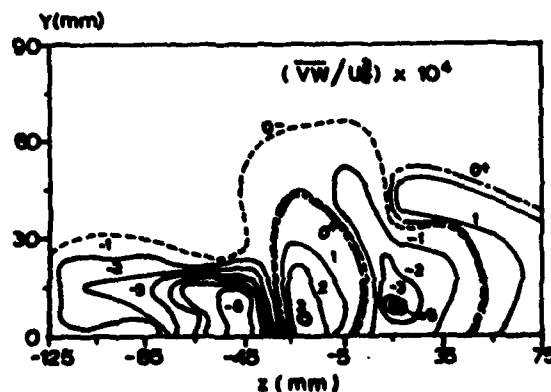

Figure 13. Secondary shear stress contours
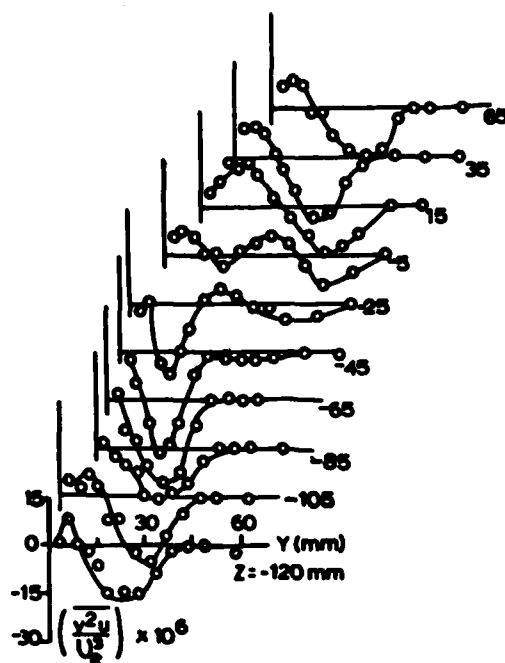

Figure 14. Cross sectional shear stress contours

Figure 15. Profiles of triple product $\overline{uv^2}$
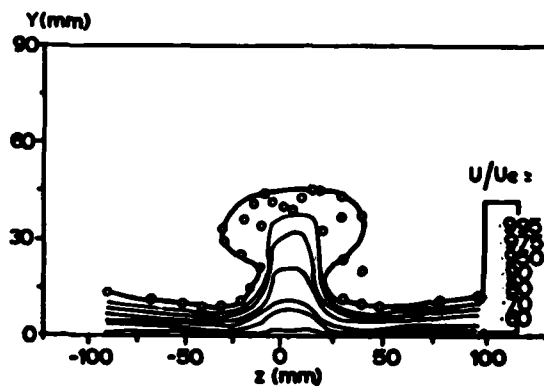

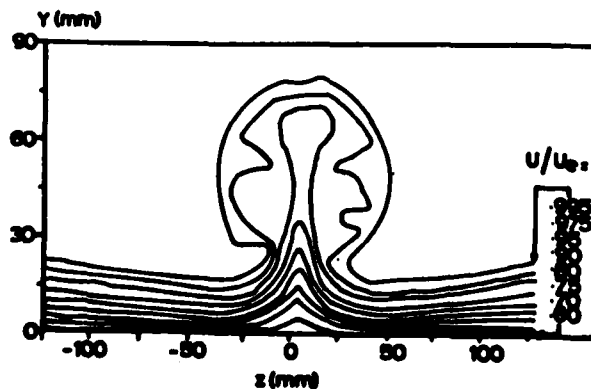Figure 16. Mean velocity contours in vortex pair at x=600 mm

Figure 17. Mean velocity contours in vortex pair at x=1350 mm

Analysis of the results of this experiment is still in progress. It extends the mean-flow measurements of Tanaka and Suzuki (4) and the old NPL results quoted by Pearcey (see Ref.5).

3.3 Vortex pair on flat surface ("common flow" outwards)

Figure 16 and 17 show mean velocity contours for this case. Figure 16 shows measurements near the front of the working section, the large scatter in the points for the U/Ue=0.995 contour being mainly a consequence of the complicated total pressure pattern in the residue of the wake of the twin-delta vortex generators in the settling chamber. In Fig. 17, the outermost contour is smooth, but the contour for U/Ue=0.975 is irregular, with some suggestion that the irregularities are real rather than just scatter in a region of small gradients. In general, the contours in these figures are plausible and accurately symmetrical, albeit about a value of z slightly different from zero. Figure 18 shows skin friction values at different streamwise stations. Again, the curves are accurately symmetrical, the dip at the centreline being the obvious result of inflow of low momentum fluid from positive and negative z . The double minimum at the smallest value of x , corresponding to the dip in the velocity contour nearest the wall (Fig. 16) is evidently a result of the disturbances caused by the vortex generators because only a single minimum is found at stations further downstream. Hot-wire measurements for this flow are in progress, and will be followed by measurements in a vortex pair with the opposite sign of rotation, so that the "common flow" is towards the surface.
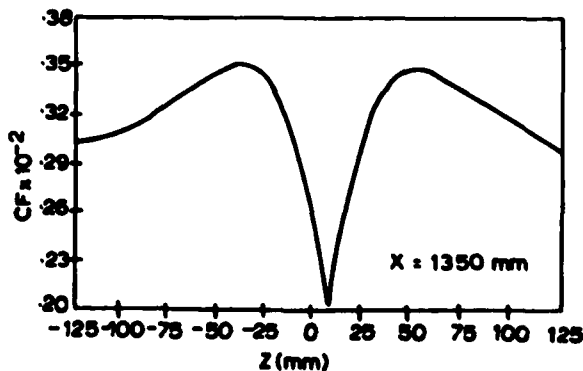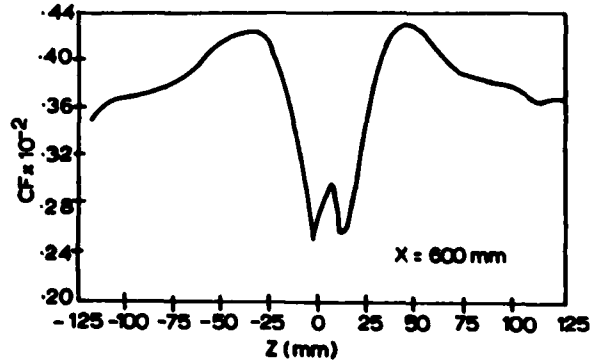

Figure 18. Skin friction coefficient below vortex pair.

4.   Conclusions

Even in their present incomplete state, the results of these experiments on longitudinal vortices imbedded in turbulent boundary layers call attention to many interesting features of the flows, in which the qualitative obviousness of the mean velocity contours conceals a great deal of non-obvious turbulence behaviour, which will have to be better understood if the mean velocity contours are to be predicted quantitatively . Longitudinal imbedded vortices are such a common feature of three-dimensional turbulent flows that serious attempts to develop a calculation method are long overdue. The results indicate that methods using eddy viscosity or eddy diffusivity are unlikely to be satisfactory, but even transport equation methods cannot be expected to reproduce all the details of the complicated profiles of Reynolds stresses shown above. The simple configurations tested in the present experiments correspond to a rather wide variety of real life flows, of importance in such diverse fields as turbomachinery, aeronautical aerodynamics, ship hydrodynamics, and internal flows.

References

1. Shabaka, I.M.M.A. "Turbulent Flow in a Simulated Wing-Body Junction", PhD thesis, Imperial College, London Univ., 1978

2. Shabaka, I.M.M.A. and Bradshaw, P. "Turbulent Flow Measurements in an Idealized Wing-Body Junction", synoptic to appear in AIAA.J.

3. Kline, S.J. et al.(Eds) Proceedings, 1980/81 AFOSR/HTTM-Stanford Conference on Complex Turbulent Flows, Vol. 1. Thermosciences Divn., Stanford Univ., 1980

4. Tanaka, I. and Suzuki, T. "Interaction Between the Boundary Layer and Longitudinal Vortices", Proceedings, International Symposium on Ship Resistance, SSPA, Goteborg, Sweden, 1978

5. Lachmann, G.V.(Ed.) Boundary Layer and Flow Control, Pergamon, Oxford, 1961, p.1277

DISTRIBUTION LIST FOR UNCLASSIFIED
TECHNICAL REPORTS AND REPRINTS ISSUED UNDER
CONTRACT _____ TASK NR 061-25.

All addresses receive one copy unless otherwise specified

Technical Library
Building 313
Ballistic Research Laboratories
Aberdeen Proving Ground, MD 21005

Dr. F. D. Bennett
External Ballistic Laboratory
Ballistic Research Laboratories
Aberdeen Proving Ground, MD 21005

Mr. C. C. Hudson
Sandia Corporation
Sandia Base
Albuquerque, NM 81115

Professor P. J. Roache
Ecodynamics Research
   Associates, Inc.
P. O. Box 8172
Albuquerque, NM 87108

Dr. J. D. Shreve, Jr.
Sandia Corporation
Sandia Base
Albuquerque, NM 81115

Defense Documentation Center
Cameron Station, Building 5
Alexandria, VA 22314   12 copies

Library
Naval Academy
Annapolis, MD 21402

Director, Tactical Technology Office
Defense Advanced Research Projects
   Agency
1400 Wilson Boulevard
Arlington, VA 22209

Office of Naval Research
Attn: Code 211
800 N. Quincy Street
Arlington, VA 22217

Office of Naval Research
Attn: Code 438
800 N. Quincy Street
Arlington, VA 22217

Office of Naval Research
Attn: Code 1021P (ONRL)
800 N. Quincy Street
Arlington, VA 22217   6 copies

Dr. J. L. Potter
Deputy Director, Technology
von Karman Gas Dynamics Facility
Arnold Air Force Station, TN 37389

Professor J. C. Wu
Georgia Institute of Technology
School of Aerospace Engineering
Atlanta, GA 30332

Library
Aerojet-General Corporation
6352 North Irwindale Avenue
Azusa, CA 91702

NASA Scientific and Technical
   Information Facility
P. O. Box 8757
Baltimore/Washington International
   Airport, MD 21240

Dr. K. C. Wang
Martin Marietta Corporation
Martin Marietta Laboratories
1450 South Rolling Road
Baltimore, MD 21227

Dr. S. A. Berger
University of California
Department of Mechanical Engineering
Berkeley, CA 94720

Professor A. J. Chorin
University of California
Department of Mathematics
Berkeley, CA 94720

Professor M. Holt
University of California
Department of Mechanical Engineering
Berkeley, CA 94720

Dr. H. R. Chaplin
Code 1600
David W. Taylor Naval Ship Research
   and Development Center
Bethesda, MD 20084

Dr. Hans Lugt
Code 184
David W. Taylor Naval Ship Research
    and Development Center
Bethesda, MD 20084

Dr. Francois Frenkiel
Code 1802.2
David W. Taylor Naval Ship Research
    and Development Center
Bethesda, MD 20084

Dr. G. R. Inger
Department of Aerospace Engineering
Virginia Polytechnic Institute and
    State University
Blacksburg, VA 24061

Professor A. H. Nayfeh
Department of Engineering Science
Virginia Polytechnic Institute and
    State University
Blacksburg, VA 24061

Mr. A. Rubel
Research Department
Grumman Aerospace Corporation
Bethpage, NY 11714

Commanding Officer
Office of Naval Research Branch Office
666 Summer Street, Bldg. 114, Section D
Boston, MA 02210

Dr. G. Hall
State University of New York at Buffalo
Faculty of Engineering and Applied
    Sciences
Fluid and Thermal Sciences Laboratory
Buffalo, NY 14214

Dr. R. J. Vidal
CALSPAN Corporation
Aerodynamics Research Department
P. O. Box 235
Buffalo, NY 14221

Professor R. F. Probstein
Department of Mechanical Engineering
Massachusetts Institute of Technology
Cambridge, MA 02139

Commanding Officer
Office of Naval Research Branch Office
536 South Clark Street
Chicago, IL 60605

Code 753
Naval Weapons Center
China Lake, CA 93555

Mr. J. Marshall
Code 4063
Naval Weapons Center
China Lake, CA 93555

Professor R. T. Davis
Department of Aerospace Engineering
University of Cincinnati
Cincinnati, OH 45221

Library MS 60-3
NASA Lewis Research Center
21000 Brookpark Road
Cleveland, OH 44135

Dr. J. D. Anderson, Jr.
Chairman, Department of Aerospace
    Engineering
College of Engineering
University of Maryland
College Park, MD 20742

Professor W. L. Melnik
Department of Aerospace Engineering
University of Maryland
College Park, MD 20742

Professor O. Burggraf
Department of Aeronautical and
    Astronautical Engineering
Ohio State University
1314 Kinnear Road
Columbus, OH 43212

Technical Library
Naval Surface Weapons Center
Dahlgren Laboratory
Dahlgren, VA 22448

Dr. F. Moore
Naval Surface Weapons Center
Dahlgren Laboratory
Dahlgren, VA 22448

Technical Library 2-51131
LTV Aerospace Corporation
P. O. Box 5907
Dallas, TX 75222

Library, United Aircraft Corporation
  Research Laboratories
Silver Lane
East Hartford, CT 06108

Technical Library
AVCO-Everett Research Laboratory
2385 Revere Beach Parkway
Everett, MA 02149

Professor G. Moretti
Polytechnic Institute of New York
Long Island Center
Department of Aerospace Engineering
  and Applied Mechanics
Route 110
Farmingdale, NY 11735

Professor S. G. Rubin
Polytechnic Institute of New York
Long Island Center
Department of Aerospace Engineering
  and Applied Mechanics
Route 110
Farmingdale, NY 11735

Dr. W. R. Briley
Scientific Research Associates, Inc.
P. O. Box 498
Glastonbury, CT 06033

Professor P. Gordon
Calumet Campus
Department of Mathematics
Purdue University
Hammond, IN 46323

Library (MS 185)
NASA Langley Research Center
Langley Station
Hampton, VA 23665

Professor A. Chapmann
Chairman, M chanical Engineering
  Department
William M. Rice Institute
Box 1892
Houston, TX 77001

Technical Library
Naval Ordnance Station
Indian Head, MD 20640

Professor D. A. Caughey
Sibley School of Mechanical and
  Aerospace Engineering
Cornell University
Ithaca, NY 14850

Professor E. L. Resler
Sibley School of Mechanical and
  Aerospace Engineering
Cornell University
Ithaca, NY 14850

Professor S. F. Shen
Sibley School of Mechanical and
  Aerospace Engineering
Ithaca, NY 14850

Library
Midwest Research Institute
425 Volker Boulevard
Kansas City, MO 64110

Dr. M. M. Hafez
Flow Research, Inc.
P. O. Box 5040
Kent, WA 98031

Dr. E. M. Murman
Flow Research, Inc.
P. O. Box 5040
Kent, WA 98031

Dr. S. A. Orszag
Cambridge Hydrodynamics, Inc.
54 Baskin Road
Lexington, MA 02173

Dr. P. Bradshaw
Imperial College of Science and
  Technology
Department of Aeronautics
Prince Consort Road
London SW7 2BY, England

Professor T. Cebeci
California State University,
  LongBeach
Mechanical Engineering Department
Long Beach, CA 90840

Mr. J. L. Hess
Douglas Aircraft Company
3855 Lakewood Boulevard
Long Beach, CA 90808

Dr. H. K. Cheng
University of Southern California,
  University Park
Department of Aerospace Engineering
Los Angeles, CA 90007

Professor J. D. Cole
Mechanics and Structures Department
School of Engineering and Applied
  Science
University of California
Los Angeles, CA 90024

Engineering Library
University of Southern California
Box 77929
Los Angeles, CA 90007

Dr. C. -M. Ho
Department of Aerospace Engineering
University of Southern California,
  University Park
Los Angeles, CA 90007

Dr. T. D. Taylor
The Aerospace Corporation
P. O. Box 92957
Los Angeles, CA 90009

Commanding Officer
Naval Ordnance Station
Louisville, KY 40214

Mr. B. H. Little, Jr.
Lockheed-Georgia Company
Department 72-74, Zone 369
Marietta, GA 30061

Professor E. R. G. Eckert
University of Minnesota
241 Mechanical Engineering Building
Minneapolis, MN 55455

Library
Naval Postgraduate School
Monterey, CA 93940

Supersonic-Gas Dynamics Research
  Laboratory
Department of Mechanical Engineering
McGill University
Montreal 12, Quebec, Canada

Dr. S. S. Stahara
Nielsen Engineering & Research, Inc.
510Clyde Avenue
Mountain View, CA 94043

Engineering Societies Library
345 East 47th Street
New York, NY 10017

Professor A. Jameson
New York University
Courant Institute of Mathematical
  Sciences
251 Mercer Street
New York, NY 10012

Professor G. Miller
Department of Applied Science
New York University
26-36 Stuyvesant Street
New York, NY 10003

Office of Naval Research
New York Area Office
715 Broadway - 5th Floor
New York, NY 10003

Dr. A. Vaglio-Laurin
Department of Applied Science
26-36 Stuyvesant Street
New York University
New York, NY 10003

Professor H. E. Rauch
Ph.D. Program in Mathematics
The Graduate School and University
  Center of the City University of
  New York
33 West 42nd Street
New York, NY 10036

Librarian, Aeronautical Library
National Research Council
Montreal Road
Ottawa 7, Canada

Lockheed Missiles and Space Company
Technical Information Center
3251 Hanover Street
Palo Alto, CA 94304

Commanding Officer
Office of Naval Research Branch Office
1030 East Green Street
Pasadena, CA 91106

California Institute of Technology
Engineering Division
Pasadena, CA 91109

Library
Jet Propulsion Laboratory
4800 Oak Grove Drive
Pasadena, CA 91103

Professor H. Liepmann
Department of Aeronautics
California Institute of Technology
Pasadena, CA 91109

Mr. L. I. Chasen, MGR-MSD Lib.
General Electric Company
Missile and Space Division
P. O. Box 8555
Philadelphia, PA 19101

Mr. P. Dodge
Airesearch Manufacturing Company
  of Arizona ,
Division of Garrett Corporation
402 South 36th Street
Phoenix, AZ 85010

Technical Library
Naval Missile Center
Point Mugu, CA 93042

Professor S. Bogdonoff
Gas Dynamics Laboratory
Department of Aerospace and
  Mechanical Sciences
Princeton University
Princeton, NJ 08540

Professor S. I. Cheng
Department of Aerospace and
  Mechanical Sciences
Princeton University
Princeton, NJ 08540

Dr. J. E. Yates
Aeronautical Research Associates
  of Princeton, Inc.
50 Washington Road
Princeton, NJ 08540

Professor L. Sirovich
Division of Applied Mathematics
Brown University
Providence, RI 02912

Dr. P. K. Dai (RI/2178)
TRW Systems Group, Inc.
One Space Park
Redondo Beach, CA 90278

Redstone Scientific Information Center
Chief, Document Section
Army Missile Command
Redstone Arsenal, AL 35809

U.S. Army Research Office
P. O. Box 12211
Research Triangle, NC 27709

Editor, Applied Mechanics Review
Southwest Research Institute
8500 Culebra Road
San Antonio, TX 78228

Library and Information Services
General Dynamics-CONVAIR
P. O. Box 1128
San Diego, CA 92112

Dr. R. Magnus
General Dynamics-CONVAIR
Kearny Mesa Plant
P. O. Box 80847
San Diego, CA 92138

Mr. T. Brundage
Defense Advanced Research Projects
  Agency
Research and Development Field Unit
APO 146, Box 271
San Francisco, CA 96246

Office of Naval Research
San Francisco Area Office
One Hallidie Plaza, Suite 601
San Francisco, CA 94102

Library
The RAND Corporation
1700 Main Street
Santa Monica, CA 90401

Dr. P. E. Rubbert
Boeing Aerospace Company
Boeing Military Airplane Development
  Organization
P. O. Box 3707
Seattle, WA 98124

Dr. H. Yoshihara
Boeing Aerospace Company
P. O. Box3999
Mail Stop 41-18
Seattle, WA 98124

Mr. R. Feldhuhn
Naval Surface Weapons Center
White Oak Laboratory
Silver Spring, MD 20910

Librarian
Naval Surface Weapons Center
White Oak Laboratory
Silver Spring, MD 20910

Dr. J. M. Solomon
Naval Surface Weapons Center
White Oak Laboratory
Silver Spring, MD 20910

Professor J. H. Ferziger
Department of Mechanical Engineering
Stanford University
Stanford, CA 94305

Professor K. Karamcheti
Department of Aeronautics and
  Astronautics
Stanford University
Stanford, CA 94305

Professor M. van Dyke
Department of Aeronautics and
  Astronautics
Stanford University
Stanford, CA 94305

Professor O. Bunemann
Institute for Plasma Research
Stanford University
Stanford, CA 94305

Engineering Library
McDonnell Douglas Corporation
Department 218, Building 101
P. O. Box 516
St. Louis, MO 63166

Dr. R. J. Hakkinen
McDonnell Douglas Corporation
Department 222
P. O. Box 516
St. Louis, MO 63166

Dr. R. P. Heinisch
Honeywell, Inc.
Systems and Research Division -
  Aerospace Defense Group
2345 Walnut Street
St. Paul, MN 55113

Dr. N. Malmuth
Rockwell International Science Center
1049 Camino Dos Rios
P. O. Box 1085
Thousand Oaks, CA 91360

Library
Institute of Aerospace Studies
University of Toronto
Toronto 5, Canada

Professor W. R. Sears
Aerospace and Mechanical Engineering
University of Arizona
Tucson, AZ 85721

Professor A. R. Seebass
Department of Aerospace and Mechanical
  Engineering
University of Arizona
Tucson, AZ 85721

Dr. K. T. Yen
Code 3015
Naval Air Development Center
Warminster, PA 18974

Air Force Office of Scientific Research
  (SREM)
Building 1410, Bolling AFB
Washington, DC 20332

Chief of Research and Development
Office of Chief of Staff
Department of the Army
Washington, DC 20310

Library of Congress
Science and Technology Division
Washington, DC 20540

Director of Research (Code RR)
National Aeronautics and Space
  Administration
600 Independence Avenue, SW
Washington, DC 20546

Library
National Bureau of Standards
Washington, DC 20234

National Science Foundation
Engineering Division
1800 G Street, NW
Washington, DC 20550

Mr. W. Koven
AIR 03E
Naval Air Systems Command
Washington, DC 20361

Mr. R. Siewert
AIR 320D
Naval Air Systems Command
Washington, DC 20361

Technical Library Division
AIR 604
Naval Air Systems Command
Washington, DC 20361

Code 2627
Naval Research Laboratory
Washington, DC 20375

SEA 03512
Naval Sea Systems Command
Washington, DC 20362

SEA 09G3
Naval Sea Systems Command
Washington, DC 20362

Dr. A. L. Slafkosky
Scientific Advisor
Commandant of the Marine Corps
  (Code AX)
Washington, DC 20380

Director
Weapons Systems Evaluation Group
Washington, DC 20305

Chief of Aerodynamics
AVCO Corporation
Missile Systems Division
201 Lowell Street
Wilmington, MA 01887

Research Library
AVCO Corporation
Missile Systems Division
201 Lowell Street
Wilmington, MA 01887

AFAPL (APRC)
AB
Wright Patterson, AFB, OH 45433

Dr. Donald J. Harney
AFFDL/FX
Wright Patterson AFB, OH 45433